Journal Pre-proof

Pyrido[2,3-b][1,5]benzoxazepin-5(6H)-one derivatives as CDK8 inhibitors

Sonia Martínez-González, Ana Belén García, M. Isabel Albarrán, Antonio Cebriá, Adrián Amezquita-Alves, Francisco Javier García-Campos, Jaime Martínez-Gago, Jorge Martínez-Torrecuadrada, Inés Muñoz, Carmen Blanco-Aparicio, Joaquín Pastor

PII: S0223-5234(20)30414-1

DOI: https://doi.org/10.1016/j.ejmech.2020.112443

Reference: EJMECH 112443

To appear in: *European Journal of Medicinal Chemistry*

Received Date: 11 March 2020

Revised Date: 7 May 2020

Accepted Date: 7 May 2020

Please cite this article as: S. Martínez-González, Ana.Belé. García, M.I. Albarrán, A. Cebriá, Adriá. Amezquita-Alves, F.J. García-Campos, J. Martínez-Gago, J. Martínez-Torrecuadrada, Iné. Muñoz, C. Blanco-Aparicio, Joaquí. Pastor, Pyrido[2,3-b][1,5]benzoxazepin-5(6H)-one derivatives as CDK8 inhibitors, *European Journal of Medicinal Chemistry* (2020), doi: https://doi.org/10.1016/j.ejmech.2020.112443.

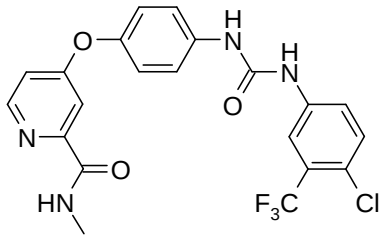

Sorafenib

CDK8 IC_{50} = 36.6 nM / P-STAT1 IC_{50} > 10 µM

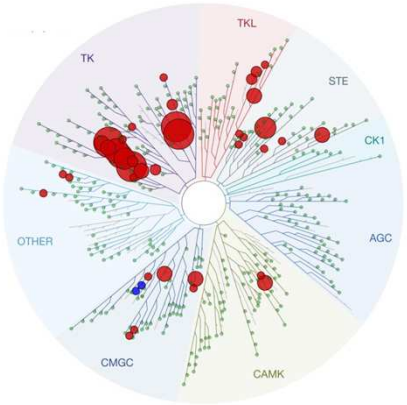

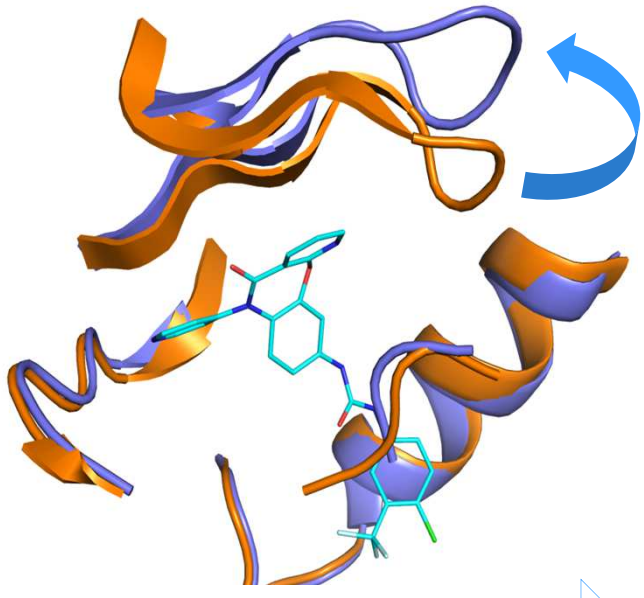

P-Loop displacement

KINOME*scan*®

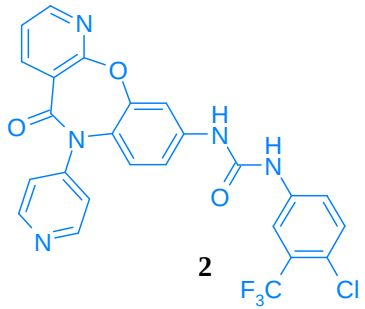

2

CDK8 IC_{50} = 8.25 nM / P-STAT1 IC_{50} = 1.3 µM

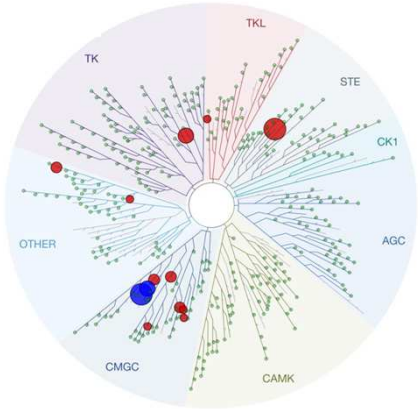

Pyrido[2,3-b][1,5]benzoxazepin-5(6H)-one Derivatives as CDK8 Inhibitors

Sonia Martínez-González[a], *Ana Belén García*[a], *Mª Isabel Albarrán*[a], *Antonio Cebriá*[a], *Adrián Amezquita-Alves*[a], *Francisco Javier García-Campos*[a], *Jaime Martínez-Gago*[b], *Jorge Martínez-Torrecuadrada*[b], *Inés Muñoz*[b], *Carmen Blanco-Aparicio*[a], *Joaquín Pastor*[a,*]

[a]Experimental Therapeutics Programme, Spanish National Cancer Research Centre (*CNIO*), C/ Melchor Fernández Almagro 3, E-28029 Madrid, Spain

[b]Crystallography and Protein Engineering Unit, Spanish National Cancer Research Centre (*CNIO*), C/ Melchor Fernández Almagro 3, E-28029 Madrid, Spain

Corresponding Author

[*] Joaquín Pastor. Phone: +34 917328000, fax: +34 917328051. E-mail address: jpastor@cnio.es.

Present addresses

Abstract

CDK8 is a cyclin-dependent kinase that forms part of the mediator complex, and modulates the transcriptional output from distinct transcription factors involved in oncogenic control. Overexpression of CDK8 has been observed in various cancers, representing a potential target for developing novel CDK8 inhibitors in cancer therapeutics. In the course of our investigations to discover new CDK8 inhibitors, we designed and synthesized tricyclic pyrido[2,3-b][1,5]benzoxazepin-5(6H)-one derivatives, by introduction of chemical complexity in the multi-kinase inhibitor Sorafenib taking into account the flexibility of the P-loop motif of CDK8 protein observed after analysis of structural information of co-crystallized CDK8 inhibitors. *In vitro* evaluation of the inhibitory activity of the prepared compounds against CDK8 led us to identify compound **2** as the most potent inhibitor of the series (IC_{50} = 8.25 nM). Co-crystal studies and the remarkable selectivity profile of compound **2** are presented. Compound **2** showed moderate reduction of phosphorylation of CDK8 substrate STAT1 in cells, in line with other reported Type II CDK8 inhibitors. We propose herein an alternative to find a potential therapeutic use for this chemical series.

Keywords: CDK8, Type II inhibitors, P-loop flexibility, Selectivity, pyrido[2,3-b][1,5]benzoxazepin-5(6H)-one scaffold.

Highlights:

- Design of novel type II tricyclic CDK8 inhibitors based on Sorafenib.
- Binding of inhibitors to CDK8 by filling an unexplored cavity via displacement of its flexible P-loop.
- Potent and highly selective pyrido[2,3-b][1,5]benzoxazepin-5(6H)-one based CDK8 inhibitors.

Graphical Abstract

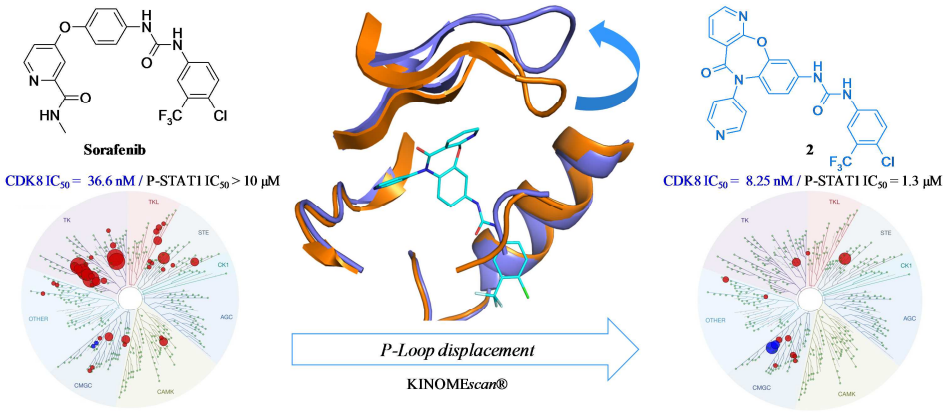

1. Introduction

CDK8 is a cyclin-dependent kinase that forms part of the mediator complex [1], which itself regulates the transcriptional activity of RNA polymerase II. There are numerous studies showing that CDK8 modulates the transcriptional output from distinct transcription factors involved in oncogenic control. These factors include the Wnt/β-catenin pathway, Notch, p53, and TGF-β [2,3]. The means by which CDK8 activity accomplishes the regulation of these various pathways remains an active area of investigation. However, it has been found that CDK8 acts as a colon cancer oncogene [4] driving Wnt pathway activity by mediating β-catenin transcriptional output. Moreover, CDK8 has been related to colorectal cancer [5], melanoma [6], and it has been demonstrated that CDK8 and its paralog CDK19 restrain increased activation of key super-enhancer-associated genes in acute myeloid leukaemia (AML) cells. Thus, CDK8/CDK19 inhibitor Cortistatin A (CA) has anti-leukaemic activity *in vitro* and *in vivo*, and induces upregulation of super-enhancers in CA-sensitive AML cell lines but not in CA-insensitive cell lines [7]. Furthermore, the phosphorylation of STAT1 at serine 727 by CDK8 is also suppressive of natural Killers (NK) cells activity. STAT1-S727-mutated NK cells display increased release of cytotoxic proteins such as granzyme B and perforin and higher cytotoxicity toward cancer cells. It suggests that CDK8 inhibition could play a role in cancer immunotherapy [8].

Several CDK8 modulators have been reported so far, among them Sorafenib [9], Senexin A and B [10], CCT251545 [11] and Cortistatin A [12]. During the last few years our group has been immersed in this field applying several approaches for hit generation towards the discovery of novel CDK8 inhibitors. Here we describe our efforts to obtain highly selective

type II CDK8 inhibitors based on Sorafenib, a known type II promiscuous inhibitor. The use of Sorafenib to design type II CDK8 inhibitors has been recently reported by other group although following a different strategy to the described herein [13]. Type II mode of inhibition, generally shows a displaced Asp-Phe-Gly (DFG) motif from a buried position in the protein to a DFG-out position, opening a "deep pocket" that can be occupied by inhibitors. In the case of CDK8, these three residues are Asp-Met-Gly (DMG) as exception to all other kinase family members [14]. In contrast to type I inhibitors that bind an activated kinase conformation, the application of inhibitors with a deep pocket binding mode is meant to target the inactive state of the enzyme.

We used the structural information of Sorafenib-bound CDK8 structure [14] (PDB 3RGF) as a basis to design our novel series of CDK8 type II inhibitors. In this X-ray structure the distal 4-pyridyl ring (N-methylpicolinamide fragment) of Sorafenib occupies the ATP adenine binding pocket of the kinase domain, interacting with the hinge region in a bidentate fashion via hydrogen bonds between the N-methylpycolinamide moiety with Ala100 backbone. The lipophilic 3-trifluoromethyl-4-chlorophenyl ring inserts into the deep pocket and establishes hydrophobic interaction with Phe176. Moreover, the C=O group of the urea functionality forms one hydrogen bond with Asp173 in the DMG triad and the corresponding NH groups form two hydrogen bonds with the glutamate side chain of Glu66, a residue that is absolutely conserved in the αC-helix of kinases. Additionally π-interactions are mapped between Sorafenib and Phe97. This binding mode of Sorafenib to CDK8/CycC is in accordance to the classical features of DFG-out binders. Unfortunately the P-loop of CDK8 is not completely solved in this structure.

The analysis of the structural information from several type II inhibitors co-crystallized with CDK8 [15], where the P-loop have been solved and defined, allowed us to identify a cavity in the ATP catalytic site flanked by side-chains of the P-loop residues Tyr32 and Val35 and those of aminoacids Ala50 and Lys52. Interestingly, the comparison of these structures indicated the high flexibility of Tyr32 depending on the nature of the inhibitor as well as some degree of flexibility of the entire P-loop (Figure S1). As a matter of example, protein structures from PDBs 4F7L and 4F6W were taken and aligned together with Sorafenib co-crystal structure 3RGF to illustrate these findings (Figure 1).

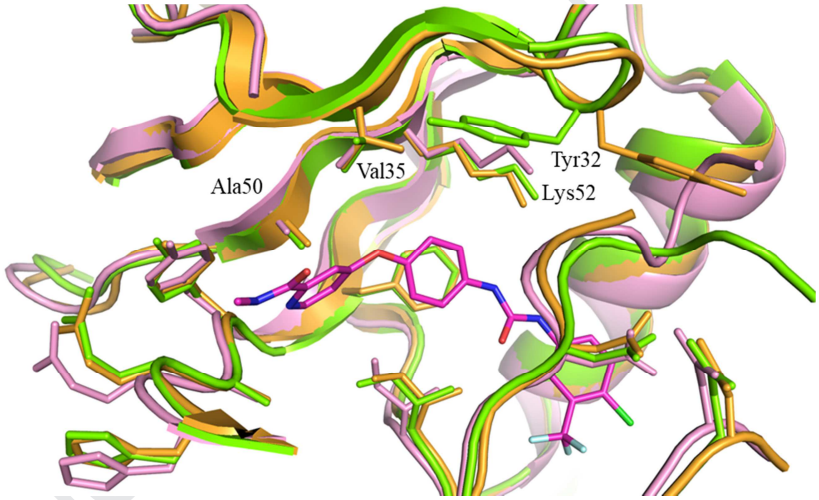

Figure 1. A close view of aligned structures 3RGF (light pink), including Sorafenib (pink C atoms), 4F7L (gold) and 4F6W (green).

We envisioned that introduction of additional chemical functionality in Sorafenib could be an interesting approach to fill such cavity in order to access unexplored and therefore novel type II CDK8 inhibitors. We designed prototype compounds **1** and **2** based on the tricyclic scaffold pyrido[2,3-b][1,5]benzoxazepin-5(6H)-one. Compound **1** contained the

hinge binding moiety N-methylpycolinamide of Sorafenib while it was replaced by pyridine in analogue **2** (Figure 2).

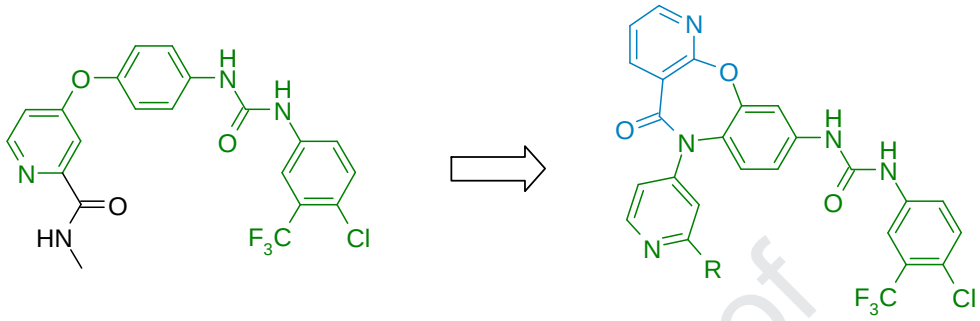

Figure 2. Design of novel type II tricyclic CDK8 inhibitors based on Sorafenib structure.

The simple alignment of the minimal energy conformation [16] of designed compound **2** with Sorafenib pointed to potential steric clashes with Val35, Lys52 and Tyr32 (inner conformation) in CDK8 structures (Figure 3). Therefore, the proposed inhibitor would need to induce a conformational change in this area of CDK8 in order to be accommodated, in particular at the level of the P-loop. As mentioned before, the observed flexibility of the P-loop, Lys52 and Tyr32 side chains in several CDK8 X-ray structures, suggested the possibility of binding of compound **2** in the catalytic site of the kinase by an induced fit mechanism**,** and therefore supported an experimental attempt to prove such hypothesis.

Furthermore, if the induced binding of compound **2** was achieved, an additional H-bond interaction could occur between the pyridine N of its scaffold and the Lys52 side chain, which is not possible in Sorafenib.

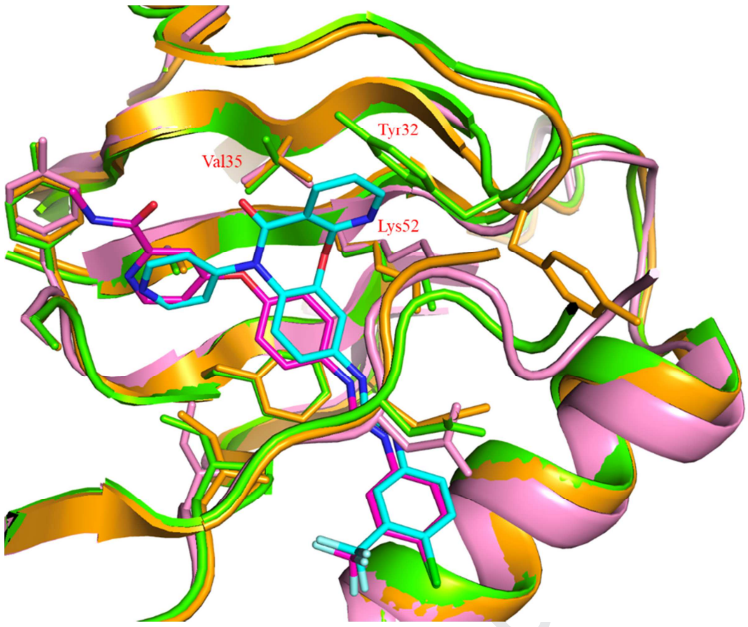

Figure 3. Alignment of designed tricyclic prototype compound **2** (cyan C-atoms) with Sorafenib (pink) using protein structures from 3RGF (light pink), 4F7L (gold) and 4F6W (green). Potential steric clashes are detected with residues Val35, Lys52 and Tyr32 (inner conformation).

2. Results and discussion

2.1. Chemistry

We focused our efforts on the preparation of compounds **1** and **2** (Scheme 1 & 2). The synthesis started from 2-hydroxynicotinic acid and 2-amino-5-nitrophenol as building blocks. In the first place, 2-hydroxynicotinic acid was converted into the corresponding acid chloride by treatment with oxalyl chloride. This intermediate was then reacted with 2-amino-5-nitrophenol to render the benzamide **3** (70% yield for the two steps). Treatment with NaOH in DMF led to the formation of the tricyclic derivative **4** with good yield (76%). Subsequent reduction of nitro group either by treatment with Fe in AcOH or by

hydrogenation with Pd/C as catalyst gave the key amino intermediate **5** in a straightforward manner with good overall yield. The amino intermediate **5** was then reacted with 4-chloro-3-(trifluoromethyl) phenyl isocyanate under standard conditions giving the urea **6a** in moderate yield (29%). Finally, coupling of cyclic amide **6a**, with 4-iodopyridine under copper catalyzed conditions rendered the desired prototype **2** albeit in low yield (9%). Attempts to obtain compound **1** from **6a** using similar coupling conditions using methyl 4-bromo-N-methylpicolinamide failed in our hands. To avoid any potential interference of the urea moiety of compound **6a** in the coupling reaction step, we decided to perform it on the intermediate **5**. Thus, reaction of **5** with 4-bromo-N-methylpicolinamide afforded compound **7a** with good yield (45%) as depicted in Scheme 2. Subsequent urea formation by reaction with 4-chloro-3-(trifluoromethyl) phenyl isocyanate gave the desired compound **1** (52% yield).

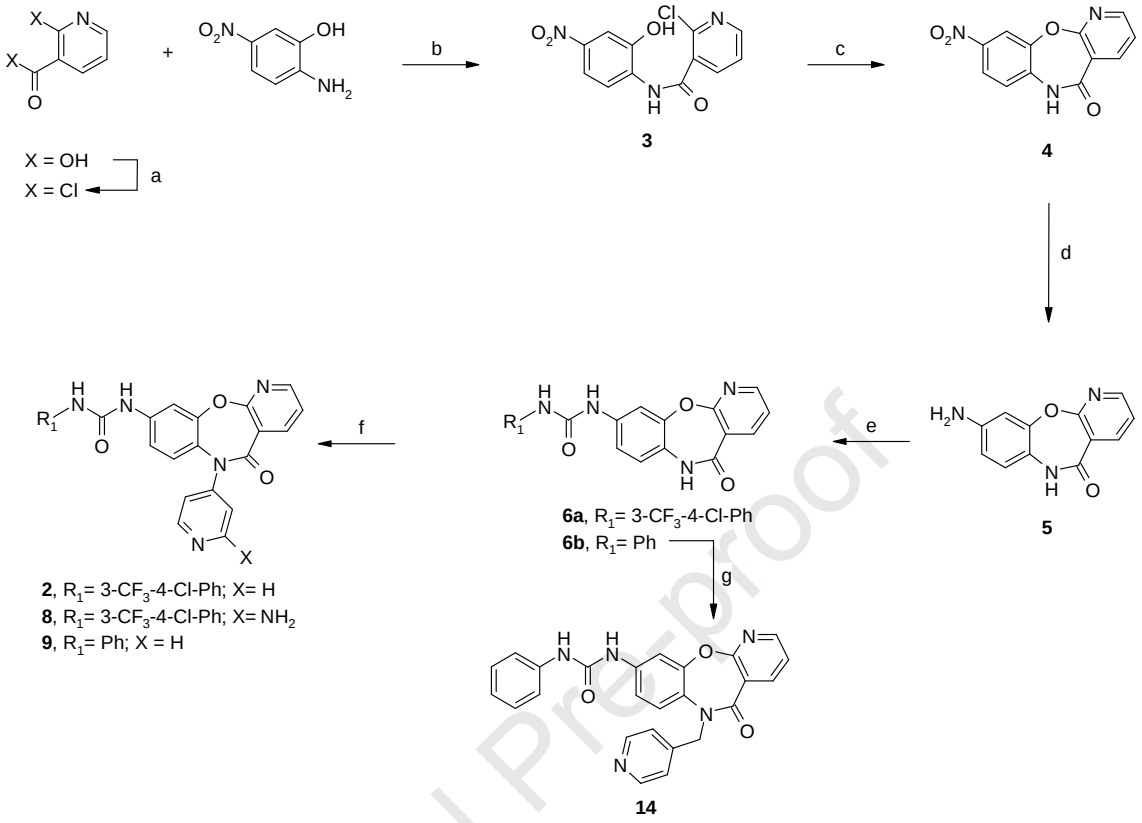

Scheme 1. Synthetic route for compound **2** and depicted analogues. Reagents and conditions: a) oxalyl chloride, CH_2Cl_2, rt, 4 h, 100%; b) DIPEA, THF, 0 ºC, 2 h, 70%; c) NaOH, DMF, 130 ºC, 90 min, 76%; d) Fe, AcOH, EtOH, H_2O, 80 ºC, 1 h, 72% or H_2, Pd/C 10 wt%, EtOH, rt, 16 h, 71%; e) R_1-isocyanate, 1,4-dioxane, 55 ºC, 2 h, ~ 30%; f) N,N'-dimethylethylendiamine, CuI, K_2CO_3, 4-halopyridine, 1,4-dioxane, 120 ºC, 24 h, ~ 10%; g) 4-(chloromethyl)pyridine hydrochloride, NaH, DMF, rt to 100 ºC, 2 h, 16%.

To the best of our knowledge, there are not previous reports of pyrido[2,3-b] [1,5]benzoxazepine-5(6H)-ones with this pattern of substitution.

Next, we explored the fragment of designed compounds targeting the deep pocket of CDK8. The urea derivatives (compounds **9–11**), amides (**16–19**) and sulfonamide (**20**)

were prepared. Originally, compound **9** was first synthesized from **5** (Scheme 1) although with rather low yield (3%). However the synthesis of **9** was significantly improved following Scheme 2 where coupling step was performed prior to the final urea formation reaction (70% yield from **5**). Based on these results we decided to apply the same synthetic procedure for the preparation of the other "deep pocket targeting analogues".

Starting from compound **5**, the 4-pyridyl analogue **7b** was obtained with 90% yield using the coupling conditions cited before. Subsequent reaction with several isocyanates rendered the final ureas **9–11** in moderate to good yield (49-89%). Sulfonamide derivative **20** was formed by reaction of **7b** with benzene sulfonyl chloride in good yield (88%) and amide derivatives **16–19** were obtained in moderate yields under standard conditions with the corresponding acid chlorides.

We also focused our efforts on the exploration of the pyridyl hinge targeting moiety. 2-aminopyridinyl fragment was introduced by copper coupling reaction of **6a** with 2-amino-4-bromopyridine to give compound **8** (Scheme 1) with low yield but in sufficient amount for biological evaluation. Compound **14** was synthesized from **6b** according to Scheme 1 by alkylation reaction with 4-(chloromethyl)pyridine in moderate yield. Other hinge targeting heteroaromatic rings were prepared from intermediate **5** by coupling reactions with 3-bromopyridine and 3-bromofurane to afford intermediate **7c-d** which rendered final compounds **12–13** after urea formation with phenyl isocyanate (Scheme 2).

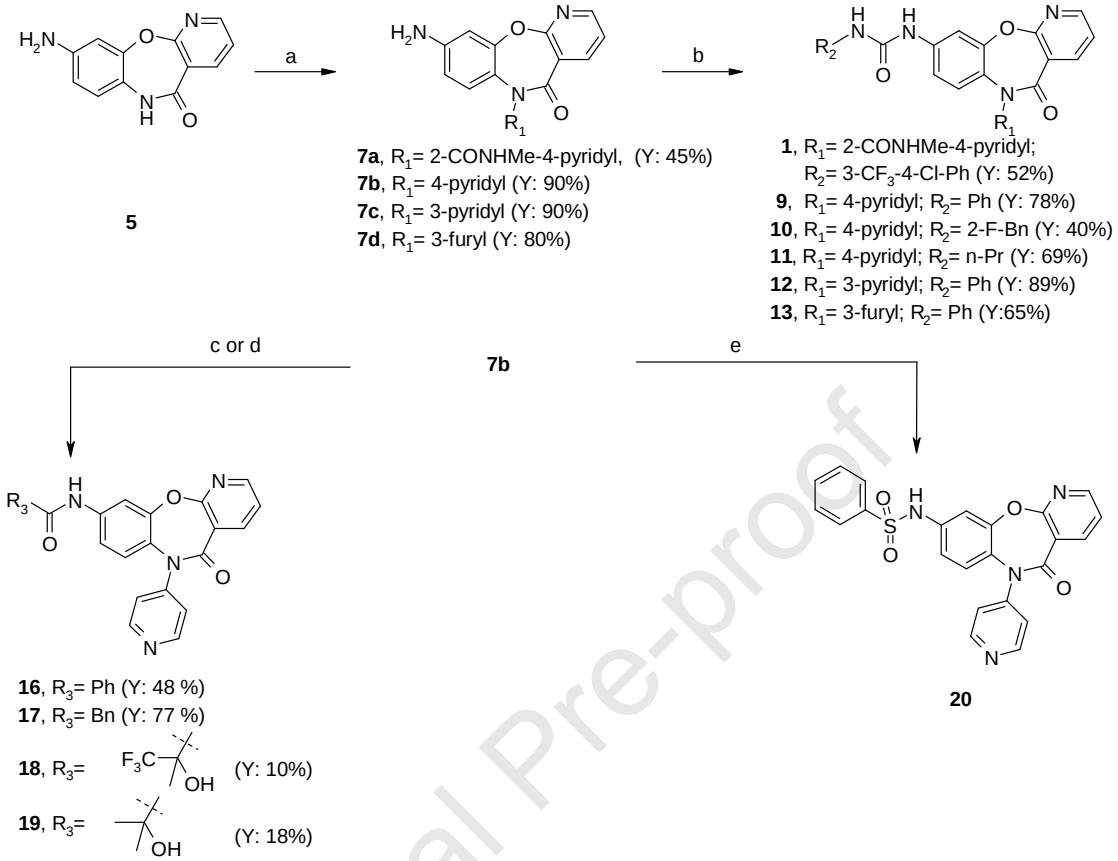

Scheme 2. Synthetic route for depicted analogues. Reagent and conditions. a) R_1Br or R_1I, CuI, N,N'-dimethylethylendiamine, Cs_2CO_3, 1,4-dioxane, 120 ºC, 20 h; b) R_2NCO, 1,4-dioxane, 55 ºC, 20 h; c) R_3COCl, K_2CO_3, 1,4-dioxane, rt, 2 h (for **16** and **17**); d) R_3CO_2H, thionyl chloride, THF, DMAc, rt, 90 min, then **7b** added, 70 ºC, 3 h (for **18** and **19**); e) benzenesulfonyl chloride, pyridine, 0 ºC, 1 h, 89%.

2.2. Biological evaluation

Next, we evaluated the inhibitory activity (IC_{50} value, half maximal inhibitory concentration) of the prepared compounds against CDK8. We were pleased to find that compound **2** displayed a potent inhibition of CDK8 with an IC_{50} in the single digit

nanomolar range (8.25 nM), about 4-fold better than Sorafenib (36.6 nM in our hands, 32.5 nM in ref. [13]). This result is the experimental proof that our hypothesis in designing this tricyclic molecule as CDK8 inhibitor was correct. Moreover, it also supports the notion that the tricyclic inhibitor **2** should induce a displacement of the P-loop in order to avoid steric clashes mentioned above and to achieve its final accommodation in the proposed binding site. Surprisingly, compound **1** displayed moderate CDK8 inhibition (IC_{50} = 361 nM). It could be explained by minor changes in the orientation of these tricyclic inhibitors in comparison with Sorafenib in the catalytic site of CDK8 rendering a not fully paralleled SAR for both classes of compounds.

Furthermore, we generated a concise SAR around these novel tricyclic CDK8 inhibitors by exploring the activity of deep pocket targeting modifications (compounds **9**–**11**) and alternative hinge binding moieties (compounds **8**, **12–14**,). The results are summarized in Table 1.

Compound **9**, with a phenyl urea fragment, demonstrated to be a potent CDK8 inhibitor (IC_{50} = 9.96 nM) in the range of compound **2**, indicating that the hydrophobic interactions made by the 3-trifluoromethyl-4-chlorophenyl ring with Phe176 in Sorafenib are still achieved with the non-substituted phenyl urea as well as the bidentate interaction of the NH groups with Glu66.

To check the size of the lipophilic cavity, the compound **10** bearing an *o*-F-benzylic urea was prepared resulting in a less potent compound with IC_{50} value of 324 nM. This result suggested that the position of phenyl ring in these molecules is important to maintain a strong inhibition against CDK8. The phenyl ring of compound **10** seems to be allocated in a less optimal position to reach the lipophilic interaction with Phe176. The aliphatic urea **11**

resulted in > 500-fold loss in potency corroborating the importance of the interactions achieved by the phenyl ring.

Table 1

CDK8 IC_{50} data for compounds **8**–**15**

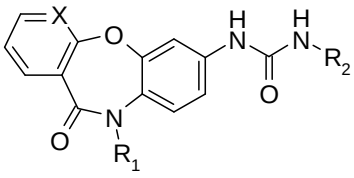

Cpd	X	R_1	R_2	CDK8 IC_{50} (nM)
8	N	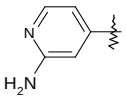	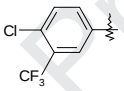	57.5
9	N			9.96
10	N		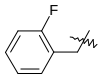	324
11	N			5060
12	N			4080
13	N			593
14	N	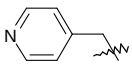		1780
15	C	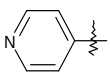		1150

Since phenyl urea **9** displayed potent activity, we next focused our efforts on the replacement of its hinge binding moiety 4-pyridine by other heteroaryls (compounds **8**, **12–14**, Table 1). The exchange of the distal 4-pyridyl by 3-pyridyl (**12**) or by a 4-pyridine homologated with a methylene spacer (**14**) decreased significantly the activity to the micromolar range (IC_{50} values of 4.08 μM and 1.78 μM respectively). The 3-furyl derivative **13**, although was better tolerated showed also a decrease in activity (IC_{50} = 593 nM). The replacement by a bidentate moiety such as 2-amino-4-pyridyl resulted in a potent compound (**8**) with an IC_{50} value of 57.5 nM. However, the comparison with compound **2** (IC_{50} =8.25 nM) demonstrated a ~ 7-fold loss of potency pointing to the impossibility of compound **8** to establish an additional interaction with the C=O backbone group of Ala100. Moreover the presence of the 2-amino group seems to weaken the interaction of the acceptor N of the pyridine moiety with the NH backbone group of the same residue.

The increase in potency of compound **2** with regard to Sorafenib and the docking studies suggested that a new interaction could be established through the N of the fused pyridine of the tricyclic scaffold and the catalytic Lys52 in CDK8. To determine its contribution we synthesized compound **15** (Scheme S1), where the pyridine was replaced by a fused phenyl ring. Interestingly, the CDK8 activity dropped to the micromolar range (Table 1) indicating that the pyridine *N* atom of the tricyclic scaffold is playing an important role for the CDK8 inhibitory activity in these pyrido[2,3-b][1,5]benzoxazepin-5(6H)-one derivatives and pointed to the establishment of an additional interaction with the protein.

Finally, we decided to replace the urea functionality (responsible for a bidentate interaction with Glu66 in Sorafenib) by other functionalities that could keep at least one of the NH groups for interaction with Glu166. The amides **16**–**19** were synthesized covering a

small range of substituents (Table 2). The benzamide **16** exhibited an IC_{50} value of 2.4 μM against CDK8, which was approximately 250 fold less potent than its urea counterpart (**9**). Similar inhibitory activity was obtained with the amide **17** which was designed with the hope that the benzylic moiety could place the phenyl ring at the same distance as it is in the potent urea **9**. We additionally incorporated a tertiary trifluoromethyl-methyl alcohol moiety previously reported as urea isostere [17, 18] in compound **18.** The corresponding methylated analogue **19** was prepared as a control for comparison purposes. The sulfonamide **20** was also synthesized. Unfortunately all these modifications (**18**–**20**) led to compounds with inhibitory activity in the micromolar range. All these results could be rationalized by the loss of the bidentate interaction of the urea group of inhibitor **9** with Glu66 and/or the impossibility to achieve the lipophilic interactions made by its phenyl ring inside the deep pocket.

Table 2

CDK8 IC_{50} activity of compounds **16**–**20**

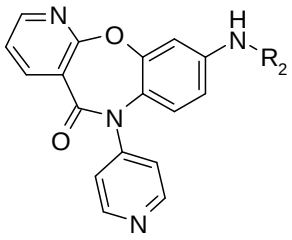

Cpd	R_2	IC_{50} (μM)	Cpd	R_2	IC_{50} (μM)
16	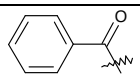	2.4	**17**	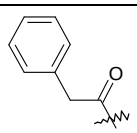	2.5

18	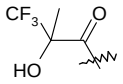	>10	**19**	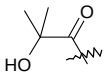	5.1
20	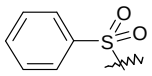	>10			

2.3. Crystal Structure

After this SAR exploration the most potent CDK8 inhibitor **2** was selected for co-crystallization studies with CDK8-CyC [19]. The crystal structure at a resolution of 2.8 Å confirmed the expected binding mode in CDK8 (Figure 4, PDB: 6TPA). The tricyclic inhibitor occupied the ATP binding site of CDK8 and prolonged the urea side chain to the typical allosteric pocket induced by classical type II inhibitors such as Sorafenib, where the protein adopted the corresponding DMG-out conformation. CDK8 inhibitor **2** established a key H-bond between the N of its 4-pyridyl moiety and the backbone NH of Ala110 in the hinge area of CDK8. Additionally, the urea portion of this molecule interacted with CDK8 by the formation of H-bonds with Glu66 side chain and Asp173 NH-backbone residue in the DMG area. On the other hand, the N of the fused pyridine of the tricyclic scaffold established another H-bond with the flexible Lys52 side chain. Moreover, a π-π interaction between Phe97 and the fused aromatic ring of its tricyclic scaffold were observed. Additional pi-sigma, pi-anion and other hydrophobic interactions between CDK8 and inhibitor **2** are established (a full detailed diagram is provided in Figure S2).

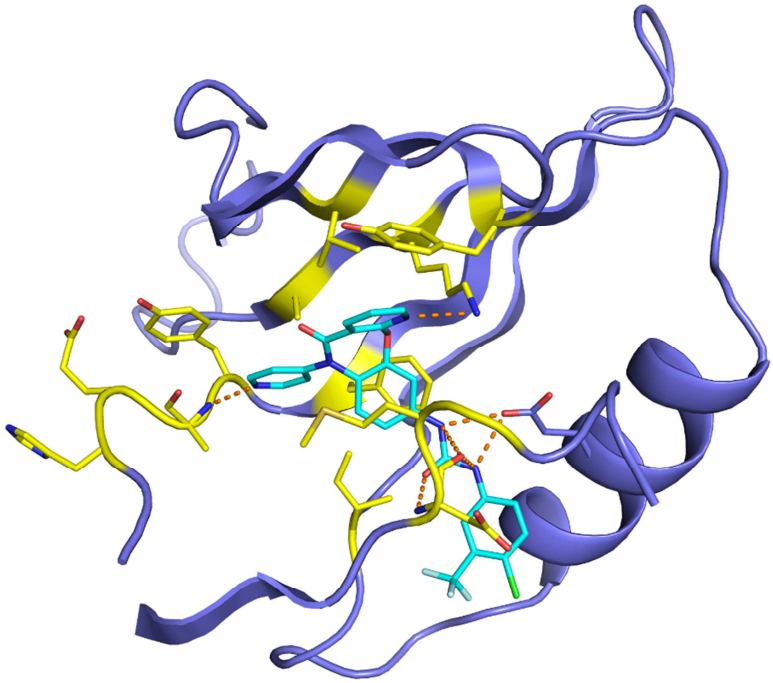

Figure 4. Close view of co-crystal structure of compound **2** and CDK8 highlighting H-bond interactions.

The co-crystal structure showed electron density in the P-loop area which allowed the resolution of its backbone as well as the orientation of the flexible Tyr32 residue. Unfortunately, the high flexibility of the P-loop did not led to a clear electron density for some side-chains, such as Val27, Arg29 and Thr31 which were introduced as glycines for crystal structure solution purposes. In spite of this, the main-chain was clear and well-defined along the whole loop.

Importantly, the accommodation of inhibitor **2** in the pocket was achieved by tilting its structure in comparison with Sorafenib to avoid the potential steric clashes suggested in Figure 1 with residues Val35 and Lys52 and by the induction of a clear displacement of the whole P-loop substructure to open the binding pocket cavity. The flexible Tyr32 residue was positioned towards the inner area of the ATP catalytic site roofing the inhibitor.

The displacement of the P-loop induced by CDK8 inhibitor **2** is remarkable in comparison with the aligned structure 4F6W in which the orientation of Tyr32 is also similar. This effect can be visualized in Figure 5.

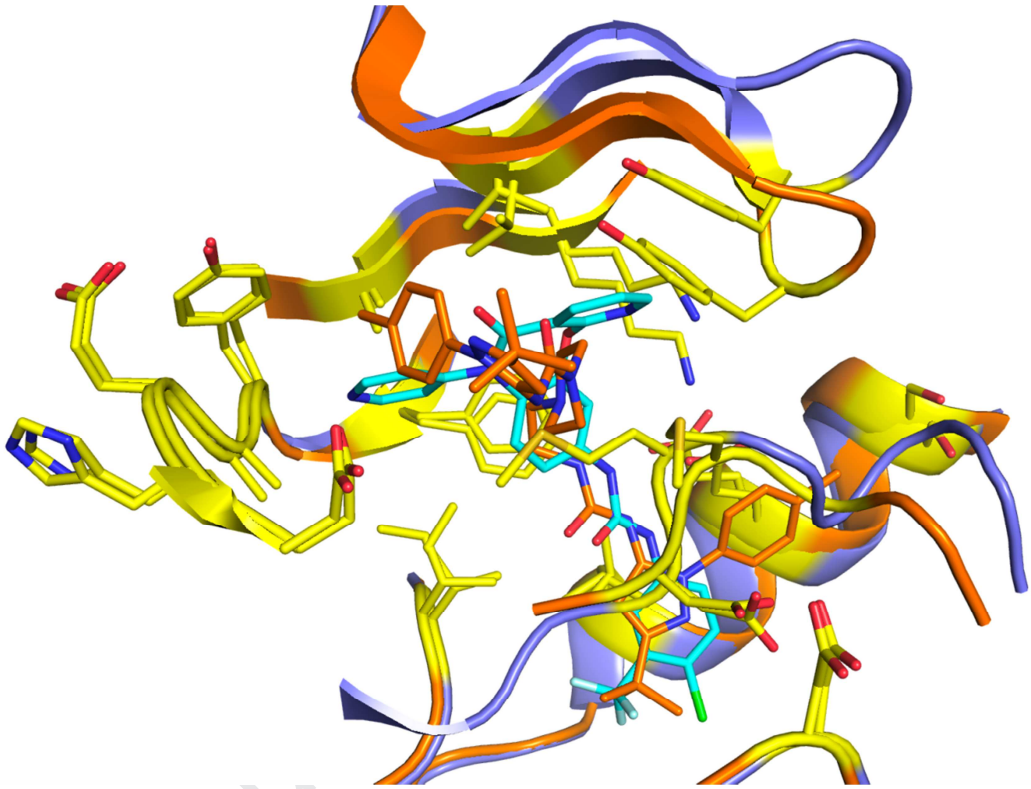

Figure 5. Close view of co-crystal structure of compound **2** and CDK8 (blue) and 4F6W and its inhibitor (orange). Key residues are highlighted to observe alignment of the proteins and the induced displacement of the P-loop by compound **2** denoted by Tyr32 position in each structure.

2.4. Selectivity

A potential effect of filling the cavity flanked by residues Tyr32-Val35-Ala50-Lys52 of CDK8 and the observed P-loop displacement induced by the designed type II class of tricyclic inhibitors could be an improvement of its on-target selectivity in comparison with

Sorafenib. It is plausible that the additional fused ring systems of these compounds could impair their binding to a wider number of kinases than the more adaptable "monocyclic Sorafenib". In order to assess this hypothesis, compound **2** was screened at 1.0 μM concentration (~150 fold higher than its IC_{50} against CDK8) in a panel of 456 kinases using a high-throughput competition binding assay (KINOME*scan*™). Compound **2** exhibited a signal below 35% of the produced by the untreated controls in this assay (a value widely accepted for a significant binding in this platform) for only 13 kinases: CDK8 and its paralog CDK19 (also named CDK11), CDK7, CLK2, CLK4, DDR1, ERK8, HIPK4, IRAK1, IKKα, JNK2, LOK and PLK3. The complete data set is provided in Table S1 in supplementary material. The calculated selectivity score S(35) of compound **2** is 0.03, indicating a high level of selectivity for a kinase inhibitor [20].

To easily visualize these results, the TREEspot™ interaction map is given (Figure 6A), which represents each kinase activity versus control after incubation with compound **2**.

Furthermore, inhibitor **2** was profiled internally against CDK19 and the off-targets CDK7, CLK4 and DDR1 in dose response experiments using orthogonal assays for validation purposes. As expected, compound **2** demonstrated a potent activity against CDK19 (IC_{50} = 29 nM), due to the high homology degree between both paralogs. Interestingly, compound **2** displayed negligible activity against CDK7 and CLK4 (IC_{50} > 10 μM) and moderated DDR1 inhibition (IC_{50} = 0.180 μM).

The promising kinase selectivity results of inhibitor **2** prompted us to compare them with those of Sorafenib. A similar broad kinase selectivity profiling for Sorafenib using KINOME*scan*™ platform was published using the inhibitor at 10 μM concentration [21]. However, for a direct comparison with compound **2**, we screened Sorafenib at the same

concentration (1 μM) in the same platform against a panel of 468 kinases (Figure 6B, Table S2). Sorafenib exhibited a selectivity score S(35) of 0.1 and 41 kinases (including CDK8 and CDK19) showed a signal below 35% of the produced by the untreated controls in this assay. Two of these kinases were not included in the original panel of 456 kinases of compound **2**. After a comparative analysis, it was reasonable to conclude that inhibitor **2** was significantly more selective for CDK8/19 than Sorafenib, the origin of its design. Therefore, the presence of the tricyclic pyrido[2,3-b][1,5]benzoxazepin-5(6H)-one scaffold had a beneficial impact for its selectivity, although contributions of the hinge binding moieties in **2** (4-pyridyl) and Sorafenib (2-picolinamide) cannot be ruled out.

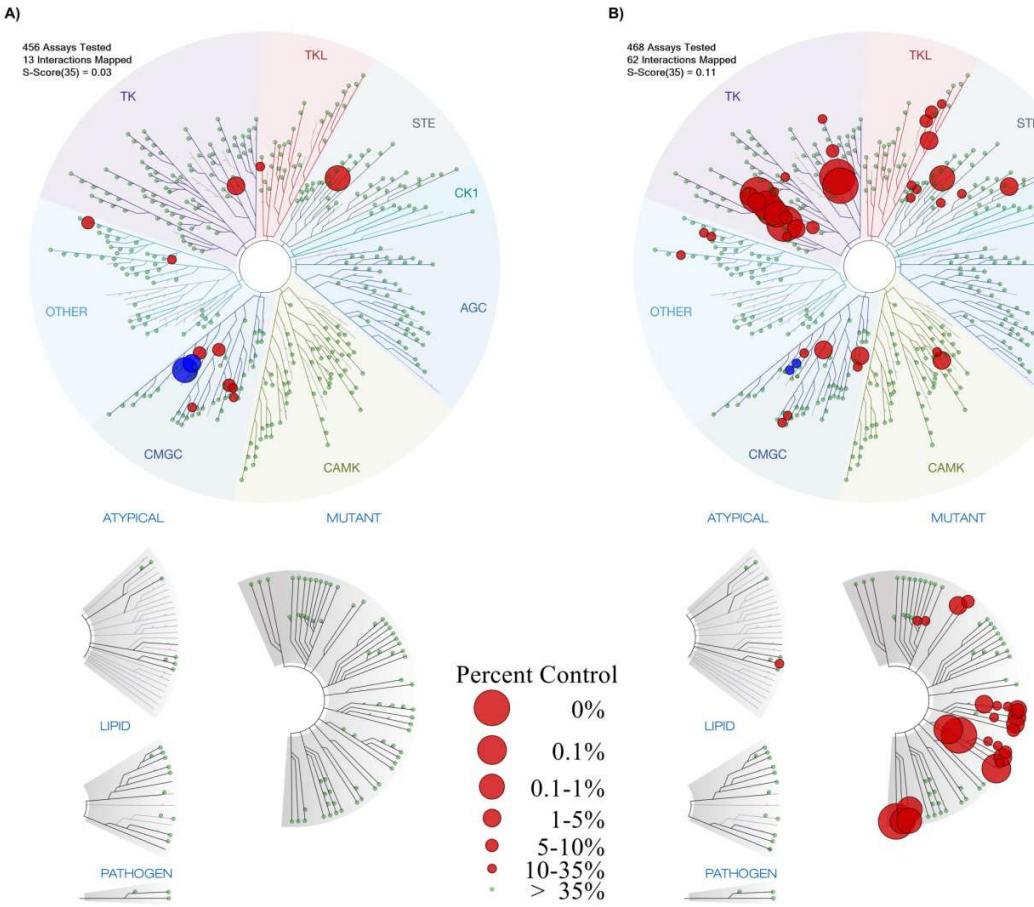

Figure 6. Selectivity profile of A) compound **2** and B) Sorafenib. Kinases found to bind (percent of control <35) are marked with red circles, where larger circles indicate higher-affinity binding. CDK8 and CDK19 are highlighted in blue color. Image generated using TREE*spot*™ Software Tool and reprinted with permission from KINOME*scan*®, a division of DiscoveRx Corporation, © DISCOVERX CORPORATION 2010.

2.5. Cellular activity

Next, we examined the modulation of phospho-STAT1^{Ser727} in cells as an *in vivo* biomarker for CDK8 inhibition [22], by our inhibitors (**2**, **8** and **9**) and Sorafenib. We only observed modulation of STAT1 phosphorylation in SW620 cells following 8 h treatment with compound **2**, showing moderate inhibition (IC_{50} = 1.3 μM; maximum inhibition of ~ 60% at 10 μM) whereas compound **8**, **9** and Sorafenib showed negligible activity (IC_{50} > 10 μM) (Figure S3).

In spite of the good biochemical activity, these compounds and Sorafenib presented disappointing CDK8 cellular activity. Our results were in line with those reported previously for other type II CDK8 inhibitors [11,13] where a similar and strong disconnection between biochemical and cellular CDK8 inhibition was observed. The explanation of this behavior was based on the notion that the inactive form of CDK8 targeted by this type of inhibitors was poorly available in cells. A very recent article [23] describes the molecular mechanism by which CDK8 is blocked in its DMG in (active) conformation when is part of the mediator complex due to its association with MED12. The preference for a DMG-in conformation of the active site disfavors type II kinase inhibitors

from binding and inhibiting CDK8 in ternary CDK8/Cyclin C/MED12 complexes, which are present in cells [23].

We alternatively determined the cellular inhibition of the off-target DDR1 kinase by compound **2**. Interestingly, **2** was able to block collagen induced DDR1 autophosphorylation in transfected HEK293T cells with DDR1 (IC_{50} p-DDR1 value of 170 nM, Figure S4). This result triggered the possibility of positioning the pyrido[2,3-b][1,5]benzoxazepin-5(6H)-one derivatives as starting points to develop novel cell active DDR1 inhibitors. As a matter of information, DDR1 kinase is involved in several diseases such as cancer (tumor progression and metastasis), lung and liver fibrosis, glomerulonephritis and atheroesclerosis among others [24].

3. Conclusions

Tricyclic pyrido[2,3-b][1,5]benzoxazepin-5(6H)-one derivatives were designed, synthesized and evaluated for their activity towards CDK8. This led to the identification of the most potent inhibitor of the series, compound **2** with IC_{50} of 8.25 nM, 4-fold more potent than Sorafenib, the compound used for its design. Moreover, compound **2** showed a remarkable selectivity over a panel of 456 kinases. Co-crystal studies showed similar binding mode than Sorafenib, with the induction of displacement of P-loop to accommodate compound **2** in the ATP cavity. It has been demonstrated that rational modifications of the scaffold of the multi-kinase inhibitor Sorafenib leading to tricyclic pyrido[2,3-b][1,5]benzoxazepin-5(6H)-one derivatives, exemplified by compound **2**, is an attractive strategy to improve its CDK8 kinase activity and selectivity. Unfortunately, and in line with other reported type II CDK8 inhibitors, the novel compounds were unable to strongly modulate the activity of CDK8 in cells. Last but not least, the promising

biochemical and cellular activity against DDR1 of representative compound **2** would allow its use as starting point to develop new DDR1 inhibitors.

4. Experimental section

4.1. General Procedures

All reagents and solvents were purchased from commercial sources and were used without further purification. ^{1}H NMR spectra were recorded at 300 or 700MHz and ^{13}C NMR at 75MHz using Bruker instruments operating at indicated frequencies. Chemical shifts are given in ppm relative to DMSO-d_6 residual peak (^{1}H, 2.50 ppm; ^{13}C, 39.51 ppm). The following abbreviations are used for the description: br = broad, s = singlet, d = doublet, dd = doublet of doublets, t = triplet, q = quartet, m = multiplet. Purification by silica flash chromatography was performed using automated Biotage systems with pre-packed cartridges. Chemical purities for final compounds were > 95% measured by LC/MS analysis at UV (254 nm), Gemini-NX C18 (100 x 2.0 mm; 5μm), Solvent A: water with 0.1% formic acid; Solvent B: acetonitrile with 0.1% formic acid. Gradient: 5% of B to 100% of B within 8 min at 50 ºC on Agilent 1200/6120 Quadrupole system. Purifications by preparative HPLC were performed on Agilent 1100; HT Zorbax SB-C18 (100 x 2.12 mm; 5μm) with appropriate gradient (solvent A: water with 0.1% formic acid; Solvent B: acetonitrile with 0.1% formic acid). Other abbreviations used along the document: rt = room temperature, DCM = dichloromethane, DMAc = dimethylacetamide, DMF = N,N-dimethylformamide, THF = tetrahydrofuran, Ar = Argon, eq = equivalent, Rt = retention time, TLC = thin layer chromatography.

4.1.1. Synthesis of compounds following Scheme 1.

*4.1.1.1. 2-Chloro-N-(2-hydroxy-4-nitro-phenyl)-nicotinamide (**3**)*

2-Hydroxynicotinic acid (4 g, 17.97 mmol) was suspended in dichloromethane (115 mL) and DMF (1.15 mL) and then oxalyl chloride (2M in CH_2Cl_2 solution, 3 eq, 43 mL) was added slowly under Ar flow (gas evolved). The mixture was stirred at rt till completion of reaction by LC-MS, 4 h. The reaction mixture was concentrated under vacuum and further dried in vacuum pump. The crude product, 2-chloronicotinoyl chloride, was used in next step assuming quantitative yield. A suspension of 2-chloronicotinoyl chloride (3.16 g, 17.95 mmol) in THF (72 mL) was added to a mixture of 2-amino-5-nitrophenol (1.15 eq, 3.18 g) and DIPEA (1.7 eq, 5.3 mL) in THF (72 mL) at 0 ºC. The reaction mixture was stirred at 0 ºC for 2 h and then allowed to get rt. The solids in suspension were filtered out and washed with ethyl acetate. The filtrate was washed with water and brine. The organic layer was dried (Na_2SO_4) and concentrated to render a solid that was triturated with CH_2Cl_2 affording **3** (brownish solid, 3.76 g, 70%); ^{1}H NMR (700 MHz, DMSO) δ 8.68 (dd, J = 4.7, 2.0 Hz, 1H), 8.64 (m, 1H), 8.10 (d, J = 2.5 Hz, 1H), 7.97 (dd, J = 9.1, 2.5 Hz, 1H), 7.67 (m, 1H), 6.85 (m, 3H). LCMS (ESI): m/z 212 $[M+ H]^+$; Rt: 4.05 min.

*4.1.1.2. 7-Nitro-10H-5-oxa-4,10-diaza-dibenzo[a,d]cyclohepten-11-one (**4**)*

Intermediate **3** (3.74 g, 12.74 mmol) was dissolved in DMF (85 mL) and NaOH (1.5 eq, 2.76 g, powdered pellets) was added. The mixture in pressure tube was heated at 120 ºC for 90 min. The reaction mixture was poured into ice-water. The solid was filtered, washed with water and triturated with methanol-Et_2O to render compound **4** (off-white solid, 2.1 g, pure required product). From the mother liquor, another batch of product precipitated which was filtered and washed with water affording 400 mg of pure compound **4** (total amount 2.5 g, 76%); ^{1}H NMR (700 MHz, DMSO) δ 11.30 (s, 1H), 8.57 (dd, J = 4.7, 2.0 Hz, 1H), 8.31

(dd, J = 7.5, 1.9 Hz, 1H), 8.15 (dd, J = 8.8, 2.5 Hz, 1H), 8.11 (d, J = 2.5 Hz, 1H), 7.53 (dd, J = 7.5, 4.8 Hz, 1H), 7.40 (d, J = 8.8 Hz, 1H); LCMS (ESI): m/z 258 $[M+ H]^+$, Rt: 3.48 min.

*4.1.1.3. 7-Amino-10H-5-oxa-4,10-diaza-dibenzo[a,d]cyclohepten-11-one (**5**)*

Intermediate **4** (2.05 g, 7.97 mmol) was suspended in ethanol (80 mL) and Pd/C 10% wt (400 mg) was slowly added. Then, hydrogen balloon was connected to the reaction mixture and it was stirred at rt. After 3 h more Pd/C was added (100 mg) and the mixture was stirred overnight. The reaction mixture was diluted with ethanol and refluxed for 2 h (in order to dissolve maximum amount of product) and then it was filtered through Watsman® paper. The filtrate was concentrated to afford pure compound **5** (pale brown solid, 1.29 g, 71%); ^{1}H NMR (300 MHz, DMSO) δ 10.30 (s, 1H), 8.46 (dd, J = 4.8, 2.0 Hz, 1H), 8.21 (dd, J = 7.6, 2.1 Hz, 1H), 7.42 (dd, J = 7.6, 4.8 Hz, 1H), 6.82 (d, J = 8.5 Hz, 1H), 6.51 (d, J = 2.4 Hz, 1H), 6.39 (dd, J = 8.5, 2.4 Hz, 1H), 5.24 (s, 2H); LCMS (ESI): m/z 228 $[M+ H]^+$, Rt: 0.8 min. When the reaction was performed at scale below 1 g, the next conditions also worked well: Intermediate **4** (1 eq, 400 mg, 1.55 mmol) was suspended in EtOH-H_2O 1:1 (15 mL) and then Fe (5 eq, 434 mg) and acetic acid (1.5 eq, 0.14 mL) were added. The mixture was heated at 80 ºC for 1 h. The reaction mixture was filtered through Celite® and rinsed thoroughly with methanol. The filtrate was concentrated and triturated with methanol rendering the compound **5** (255 mg, 72%). Removal of iron salts from the low soluble required product was difficult and messy at scale bigger than 1 g.

*4.1.1.4. 1-(4-Chloro-3-trifluoromethyl-phenyl)-3-(11-oxo-10,11-dihydro-5-oxa-4,10-diaza-dibenzo[a,d]cyclohepten-7-yl)-urea (**6a**)*

Intermediate **5** (550 mg, 2.42 mmol) was suspended in 1,4-dioxane (20 mL) and 4-chloro-3-(trifluoromethyl)phenyl isocyanate (536 mg, 2.42 mmol) was added. The mixture

under Ar atmosphere was heated at 55 ºC for 2 h. The mixture was concentrated on Celite® and loaded into flash silica column. Elution with gradient c-Hex-EtOAc 25-100% of EtOAc afforded compound **6a** (white solid, 315 mg, 29%); ^{1}H NMR (300 MHz, DMSO) δ 10.65 (s, 1H), 9.22 (s, 1H), 9.02 (s, 1H), 8.51 (m, 1H), 8.27 (m, 1H), 8.10 (s, 1H), 7.63 (s, 3H), 7.46 (dd, J = 7.5, 4.9 Hz, 1H), 7.21 (d, J = 8.8 Hz, 1H), 7.10 (d, J = 8.7 Hz, 1H); LCMS (ESI): m/z 449 $[M+ H]^+$, Rt: 4.48 min.

*4.1.1.5. 1-(11-Oxo-10,11-dihydro-5-oxa-4,10-diaza-dibenzo[a,d]cyclohepten-7-yl)-3-phenyl-urea (**6b**)*

Intermediate **5** (32 mg, 0.141 mmol) was suspended in dichloromethane (1.5 mL) and phenyl isocyanate (1.1 eq, 17 μL) was added. The mixture was stirred at rt for 28 h and then more isocyanate (1.5 eq, 23 μL) was added stirring for additional 96 h. The mixture was concentrated and purified by HPLC to afford compound **6b** (15 mg, white solid, 30%); ^{1}H NMR (700 MHz, DMSO) δ 10.62 (s, 1H), 8.94 (s, 1H), 8.81 (s, 1H), 8.51 (dd, J = 4.7, 2.0 Hz, 1H), 8.26 (dd, J = 7.5, 2.0 Hz, 1H), 7.66 (d, J = 2.2 Hz, 1H), 7.46 (m, 3H), 7.28 (t, J = 7.9 Hz, 2H), 7.16 (dd, J = 8.6, 2.3 Hz, 1H), 7.09 (d, J = 8.6 Hz, 1H), 6.97 (t, J = 7.3 Hz, 1H); LCMS (ESI): m/z 347.2 $[M+ H]^+$, Rt: 4.27min.

*4.1.1.6. 1-(4-Chloro-3-trifluoromethyl-phenyl)-3-(11-oxo-10-pyridin-4-yl-10,11-dihydro-5-oxa-4,10-diaza-dibenzo [a,d]cyclohepten-7-yl)-urea (**2**)*

Intermediate **6a** (75 mg, 0.167 mmol), 4-iodopyridine (1.5 eq, 51 mg) and K_2CO_3 (2.0 eq, 46 mg) were suspended in 1,4-dioxane (2 mL). Argon was bubbled into the suspension for several minutes and then, CuI (0.1 eq, 2mg) and N,N'-dimethylethylenediamine (0.2 eq, 4μL, one drop of glass pipette) were added. The reaction mixture, in pressure tube, was degassed and filled with Ar before heating at 120 ºC. After 6 h, more reactants were added

(4-iodopyridine, 20 mg; K_2CO_3, 20 mg, CuI, 2 mg, dimethylethylenediamine, 1 drop) and heating was continued up to 15 h. The reaction mixture was concentrated into Celite® and loaded into flash silica column. Elution with gradient EtOAc and MeOH from 0-5% of MeOH afforded compound **2** still impure, which was purified by preparative HPLC to render pure compound **2** (white solid, 8 mg, 9%); ^{1}H NMR (300 MHz, DMSO) δ 9.55 (s, 1H), 9.47 (s, 1H), 8.72 (s, 2H), 8.54 (dd, J = 4.8, 2.0 Hz, 1H), 8.34 (dd, J = 7.6, 1.9 Hz, 1H), 8.10 (d, J = 2.2 Hz, 1H), 7.80 (d, J = 2.3 Hz, 1H), 7.64 (m, 2H), 7.52 (m, 3H), 7.16 (dd, J = 8.9, 2.4 Hz, 1H), 6.77 (d, J = 8.8 Hz, 1H). ^{13}C NMR (75 MHz, DMSO) δ 163.42, 163.10, 152.36, 152.27, 152.11, 151.04, 148.61, 143.17, 139.06, 138.76, 132.04, 127.30, 126.24, 123.34, 123.25, 123.03, 122.66, 120.64, 116.58, 111.36. LCMS (ESI): m/z 526.1 $[M+ H]^+$, Rt: 5.03 min.

*4.1.1.7. 1-[10-(2-Amino-pyridin-4-yl)-11-oxo-10,11-dihydro-5-oxa-4,10-diaza-dibenzo[a,d] cyclohepten -7-yl]-3-(4-chloro-3-trifluorome- thyl-phenyl)-urea (**8**)*

Intermediate **6a** (50 mg, 0.111 mmol), 2-amino-4-bromopyridine (1.5 eq, 0.167 mmol, 29 mg), K_2CO_3 (2.5 eq, 38mg) and CuI (0.2 eq, 4 mg) were suspended in dioxane (1 mL). Argon was bubbled and then N,N'-dimethylethylenediamine (0.5 eq, 6 μL) was added. The reaction mixture, in pressure tube, was degassed and filled with Ar before heating at 120 ºC. After 6 h more reactants were added bromopyridine (15 mg), K_2CO_3 (20 mg) and CuI (2 mg) stirring the reaction up to 24 h. The reaction mixture was concentrated into Celite® and loaded into flash silica column. Elution with gradient EtOAc and MeOH from 0-10% of MeOH afforded compound **8** still impure, which was purified by preparative HPLC to render pure compound **8** (white solid, 5 mg, 9%); ^{1}H NMR (300 MHz, DMSO) δ 10.39 (s, 1H), 10.27 (s, 1H), 8.51 (dd, J = 4.8, 2.0 Hz, 1H), 8.29 (dd, J = 7.6, 2.0 Hz, 1H), 8.13 (d, J

= 2.4 Hz, 1H), 8.00 (d, J = 4.4 Hz, 1H), 7.78 (d, J = 2.4 Hz, 1H), 7.74 – 7.66 (m, 1H), 7.60 (d, J = 8.8 Hz, 1H), 7.50 (dd, J = 7.6, 4.8 Hz, 1H), 7.22 (dd, J = 8.9, 2.3 Hz, 1H), 6.85 (d, J = 8.9 Hz, 1H), 6.53 (dd, J = 5.4, 1.8 Hz, 1H), 6.48 (d, J = 1.5 Hz, 1H), 6.16 (s, 2H). LCMS (ESI): m/z 541.1 $[M+ H]^+$, Rt: 4.62 min.

*4.1.1.8. 1-(11-Oxo-10-pyridin-4-yl-10,11-dihydro-5-oxa-4,10-diaza-dibenzo[a,d]cyclohepten-7-yl)-3-phenyl-urea (**9**)*

Intermediate **7a** (30 mg, 0.087 mmol), 4-iodopyridine (1.25 eq, 22 mg) and K_2CO_3 (2.0 eq, 24 mg) were suspended in 1,4-dioxane (1 mL). Argon was bubbled into the suspension for several minutes and then, CuI (0.1 eq, 2 mg) and N,N'-dimethylethylenediamine (0.1 eq, 1–2μL) were added. The reaction mixture, in pressure tube, was degassed and filled with Ar and then it was heated at 120 ºC for 15 h. The reaction mixture was filtered though Celite® and washing with ethyl acetate. The filtrate was concentrated and purified by silica flash chromatography (EtOAc-MeOH from 0–5% of MeOH) affording required product that needed second purification by HPLC to render pure compound **9** (white solid, 4 mg, 10%); ^{1}H NMR (700 MHz, DMSO) δ 9.09 (s, 1H), 8.82 (d, J = 17.1 Hz, 1H), 8.71 (d, J = 5.2 Hz, 2H), 8.54 (m, 1H), 8.34 (m, 1H), 7.82 (d, J = 2.3 Hz, 1H), 7.53 (m, 3H), 7.44 (d, J = 8.0 Hz, 2H), 7.28 (t, J = 7.8 Hz, 2H), 7.08 (dd, J = 8.9, 2.3 Hz, 1H), 6.98 (t, J = 7.3 Hz, 1H), 6.77 (d, J = 8.9 Hz, 1H); LCMS (ESI): m/z 424.0 $[M+ H]^+$, Rt: 3.91min.

*4.1.1.9. 1-(11-Oxo-10-pyridin-4-ylmethyl-10,11-dihydro-5-oxa-4,10-diaza-dibenzo[a,d]cyclohepten-7-yl)-3-phenyl-urea (**14**)*

To intermediate **6b** (48 mg, 0.139 mmol) in DMF (1.4 mL) was added NaH (60% dispersion oil, 3 eq, 17 mg). After 15 min stirring at rt, 4-(chloromethyl)pyridine hydrochloride (1.5 eq, 34 mg) was added and the mixture was heated at 100 ºC for 2 h. The

mixture at rt was partitioned in ethyl acetate and water. Layers were separated and the aqueous phase was extracted twice with ethyl acetate. The combined organic layers were dried (Na_2SO_4) and concentrated to render the crude product. It was purified by flash silica chromatography (c-Hex-EtOAc 50-100% of EtOAc, then EtOAc-MeOH 95:5). Further purification by HPLC afforded pure compound **14** (white solid, 9 mg, 15%); ^{1}H NMR (700 MHz, DMSO) δ 9.06 (s, 1H), 8.88 (s, 1H), 8.51 (m, 3H), 8.28 (m, 1H), 7.71 (d, J = 2.4 Hz, 1H), 7.49 (m, 1H), 7.44 (d, J = 7.9 Hz, 2H), 7.35 (d, J = 8.9 Hz, 1H), 7.30 (d, J = 5.7 Hz, 2H), 7.27 (t, J = 7.9 Hz, 2H), 7.15 (dd, J = 8.9, 2.4 Hz, 1H), 6.97 (t, J = 7.3 Hz, 1H), 5.35 (s, 2H); LCMS (ESI): m/z 438.2 $[M+ H]^+$, Rt: 3.28min.

4.1.2. Synthesis of compounds following Scheme 2

*4.1.2.1. General procedure for N-arylation of intermediate **5** to generate intermediates **7a-d***

Intermediate **5** (1 eq), corresponding bromo or iodoheteroaryl (1.5–2 eq) and Cs_2CO_3 (2 eq) were suspended in 1,4-dioxane (0.1M). Argon was bubbled into the suspension for several minutes and then CuI (0.1 eq) and N,N'-dimethylethylenediamine (0.2 eq) were added. The reaction mixture in pressure tube was degassed and filled with Ar and then it was heated at 120 ºC for 20–24 h. The reaction mixture was filtered through Celite® washing with ethyl acetate. The filtrate was concentrated and purified by silica flash chromatography.

*4.1.2.2. 4-(7-Amino-11-oxo-11H-5-oxa-4,10-diaza-dibenzo[a,d]cyclohepten-10-yl)-pyridine-2-carboxylic acid methylamide (**7a**)*

From intermediate **5** (40 mg, 0.176 mmol) and 4-bromo-pyridine-2-carboxylic acid methyl amide following the general procedure (24 h; purification gradient: c-Hex-EtOAc 40–80% of EtOAc), compound **7a** was got (white solid, 60 mg, 94%); ^{1}H NMR (300 MHz,

DMSO) δ 8.85 (d, J = 4.8 Hz, 1H), 8.70 (d, J = 5.3 Hz, 1H), 8.50 (dd, J = 4.8, 2.0 Hz, 1H), 8.33 (dd, J = 7.6, 2.0 Hz, 1H), 8.00 (d, J = 1.8 Hz, 1H), 7.65 (dd, J = 5.3, 2.2 Hz, 1H), 7.50 (dd, J = 7.6, 4.8 Hz, 1H), 6.62 (d, J = 2.4 Hz, 1H), 6.54 (d, J = 8.7 Hz, 1H), 6.34 (dd, J = 8.7, 2.5 Hz, 1H), 5.59 (s, 2H), 2.82 (t, J = 7.7 Hz, 3H); LCMS (ESI): m/z 362 $[M+ H]^+$, Rt: 3.24 min.

4.1.2.3. 7-Amino-10-pyridin-4-yl-10H-5-oxa-4,10-diaza-dibenzo[a,d]cyclohepten-11-one ***(7b)***

From intermediate **5** (250 mg, 1.1 mmol) and 4-iodopyridine following the general procedure (24 h; purification gradient: c-Hex-EtOAc 50–100% of EtOAc), compound **7b** was got (white solid, 300 mg, 90%); ^{1}H NMR (300 MHz, DMSO) δ 8.65 (d, J = 4.5 Hz, 2H), 8.49 (s, 1H), 8.30 (d, J = 7.6 Hz, 1H), 7.47 (d, J = 10.3 Hz, 1H), 7.43 (d, J = 4.3 Hz, 2H), 6.60 (s, 1H), 6.51 (d, J = 6.5 Hz, 1H), 6.34 (d, J = 8.8 Hz, 1H), 5.55 (s, 2H); LCMS (ESI): m/z 305 $[M+ H]^+$, Rt: 0.46min and 0.96 min.

4.1.2.3. 7-Amino-10-pyridin-3-yl-10H-5-oxa-4,10-diaza-dibenzo[a,d]cyclohepten-11-one ***(7c)***

From intermediate **5** (50 mg, 0.22 mmol) and 3-bromopyridine following the general procedure (20 h; purification gradient: c-Hex-EtOAc 25–100% of EtOAc) compound **7c** was got (pale yellow solid, 60 mg, 90%); LCMS (ESI): m/z 305 $[M+ H]^+$, Rt: 2.0 min.

4.1.2.4. 7-Amino-10-furan-3-yl-10H-5-oxa-4,10-diaza-dibenzo[a,d]cyclohepten-11-one ***(7d)***

From intermediate **5** (50 mg, 0.22 mmol) and 3-bromofuran following the general procedure (20 h; purification gradient: c-Hex-EtOAc 0–80% of EtOAc) the compound **7d** was got (pale yellow solid, 52 mg, 80%); LCMS (ESI): m/z 294 $[M+ H]^+$, Rt: 3.59 min.

*4.1.3. General procedure for urea formation (**1**, **9–13**)*

Intermediate **7a**–**d** (1 eq) and corresponding isocyanate (1.5 eq) in 1,4-dioxane (0.1M) were heated at 60 ºC until no starting material was detected either by TLC or by LC-MS analysis. The reaction mixture was concentrated on Celite® to be purified by silica flash chromatography or the solid in suspension was filtered and washed to render required product.

*4.1.3.1. 4-{7-[3-(4-Chloro-3-trifluoromethyl-phenyl)-ureido]-11-oxo-11H-5-oxa-4,10-diaza-dibenzo [a,d]cyclohepten-10-yl}-pyridine-2-carboxylic acid methylamide (**1**)*

From intermediate **7a** (20 mg, 0.055 mmol) and 4-chloro-3-(trifluoromethyl)phenyl isocyanate following the general procedure (4 h; purification gradient: c-Hex-EtOAc 10-100% of EtOAc), the compound **1** was isolated (white solid, 17 mg, 52%); ^{1}H NMR (300 MHz, DMSO) δ 1H NMR (300 MHz, DMSO) d 9.27 (s, 1H), 9.21 (s, 1H), 8.91 (d, J = 4.8 Hz, 1H), 8.75 (d, J = 5.3 Hz, 1H), 8.54 (dd, J = 4.8, 1.9 Hz, 1H), 8.37 (dd, J = 7.6, 1.9 Hz, 1H), 8.12 – 8.03 (m, 2H), 7.81 (d, J = 2.3 Hz, 1H), 7.68 (dd, J = 5.3, 2.1 Hz, 1H), 7.61 (dd, J = 17.1, 8.2 Hz, 2H), 7.54 (dd, J = 7.6, 4.8 Hz, 1H), 7.14 (dd, J = 8.9, 2.4 Hz, 1H), 6.80 (d, J = 8.9 Hz, 1H), 2.84 (d, J = 4.8 Hz, 3H); LCMS (ESI): m/z 583.1 $[M+ H]^{+}$, Rt: 5.72 min.

*4.1.3.2. 1-(11-Oxo-10-pyridin-4-yl-10,11-dihydro-5-oxa-4,10-diaza-dibenzo[a,d] cyclohepten-7-yl)-3-phenyl-urea (**9**)*

From intermediate **7b** (90 mg, 0.296 mmol) and phenyl isocyanate following the general procedure (2 h; purification by filtration of the solid in suspension and rinsed with water), the compound **9** was isolated (white solid, 98 mg, 78%); ^{1}H NMR (300 MHz, DMSO) δ 8.97 (s, 1H), 8.73 (s, 1H), 8.70 (dd, J = 4.6, 1.6 Hz, 2H), 8.53 (dd, J = 4.8, 2.0 Hz, 1H), 8.33 (dd, J = 7.6, 2.0 Hz, 1H), 7.82 (d, J = 2.4 Hz, 1H), 7.51 (ddd, J = 5.4, 4.5, 3.2 Hz, 3H),

7.44 (dd, J = 8.6, 1.1 Hz, 2H), 7.33 – 7.23 (m, 2H), 7.07 (dd, J = 8.9, 2.5 Hz, 1H), 6.98 (t, J = 7.3 Hz, 1H), 6.76 (d, J = 8.9 Hz, 1H); LCMS (ESI): m/z 424.1 $[M+ H]^+$, Rt: 3.73 min.

*4.1.3.3. 1-(2-Fluoro-benzyl)-3-(11-oxo-10-pyridin-4-yl-10,11-dihydro-5-oxa-4,10-diaza-dibenzo[a,d] cyclohepten-7-yl)-urea (**10**)*

From intermediate **7b** (18 mg, 0.059 mmol) and 2-fluorobenzyl isocyanate following the general procedure (24 h; purification by silica column, gradient c-Hex-EtOAc 20-100% of EtOAc), the compound **10** was obtained (white solid, 11 mg, 40%); ^{1}H NMR (300 MHz, DMSO) δ 8.93 (s, 1H), 8.72 (brs, 2H), 8.51 (dd, J = 4.8, 2.0 Hz, 1H), 8.32 (dd, J = 7.6, 2.0 Hz, 1H), 7.78 (d, J = 2.4 Hz, 1H), 7.51 (m, 3H), 7.32 (m, 2H), 7.18 (m, 2H), 7.01 (dd, J = 8.9, 2.4 Hz, 1H), 6.71 (m, 2H), 4.33 (d, J = 5.8 Hz, 2H); LCMS (ESI): m/z 456.2 $[M+ H]^+$, Rt: 3.7 min.

*4.1.3.4. 1-(11-Oxo-10-pyridin-4-yl-10,11-dihydro-5-oxa-4,10-diaza-dibenzo[a,d] cyclohepten-7-yl)-3-propyl-urea (**11**)*

From intermediate **7b** (50 mg, 0.164 mmol) and n-propyl isocyanate (several extra additions of isocyanate were needed) following the general procedure (24 h; purification by silica column, gradient DCM-MeOH from 0–5% of MeOH), the compound **11** was got (white solid, 44 mg, 69%); ^{1}H NMR (300 MHz, DMSO) δ 8.70 (m, 3H), 8.52 (dd, J = 4.8, 2.0 Hz, 1H), 8.32 (dd, J = 7.6, 2.0 Hz, 1H), 7.78 (d, J = 2.5 Hz, 1H), 7.51 (dd, J = 6.8, 4.1 Hz, 1H), 7.49 (dd, J = 4.6, 1.5 Hz, 2H), 6.99 (dd, J = 8.9, 2.5 Hz, 1H), 6.70 (d, J = 8.9 Hz, 1H), 6.21 (t, J = 5.7 Hz, 1H), 3.03 (dd, J = 12.9, 6.7 Hz, 2H), 1.43 (m, 2H), 0.86 (t, J = 7.4 Hz, 3H); ^{13}C NMR (75 MHz, DMSO) δ 163.46, 163.22, 154.90, 152.32, 150.90, 148.75, 143.10, 140.27, 126.15, 125.93, 123.14, 122.96, 120.72, 115.41, 110.11, 40.87, 22.91, 11.31. LCMS (ESI): m/z 390.6 $[M+ H]^+$, Rt: 3.10 min.

*4.1.3.5. 1-(11-Oxo-10-pyridin-3-yl-10,11-dihydro-5-oxa-4,10-diaza-dibenzo[a,d] cyclohepten-7-yl)-3-phenyl-urea (**12**)*

From intermediate **7c** (50 mg, 0.163 mmol) and phenyl isocyanate (2 eq) following the general procedure (24 h; purification by silica column, gradient c-Hex-EtOAc from 20–100% of EtOAc), the compound **12** was got (white solid, 62 mg, 89%); ^{1}H NMR (700 MHz, DMSO) δ 8.96 (s, 1H), 8.74 (s, 1H), 8.68 (d, J = 2.4 Hz, 1H), 8.61 (d, J = 3.6 Hz, 1H), 8.54 (dd, J = 4.7, 2.1 Hz, 1H), 8.34 (dd, J = 7.5, 2.0 Hz, 1H), 7.93 (m, 1H), 7.82 (d, J = 2.4 Hz, 1H), 7.58 (dd, J = 8.1, 4.8 Hz, 1H), 7.53 (m, 1H), 7.44 (d, J = 7.9 Hz, 2H), 7.28 (t, J = 7.9 Hz, 2H), 7.06 (dd, J = 8.9, 2.4 Hz, 1H), 6.98 (t, J = 7.3 Hz, 1H), 6.73 (d, J = 8.9 Hz, 1H); LCMS (ESI): m/z 424.1 $[M+ H]^{+}$, Rt: 4.62 min.

*4.1.3.6. 1-(10-Furan-3-yl-11-oxo-10,11-dihydro-5-oxa-4,10-diaza-dibenzo[a,d] cyclohepten-7-yl)-3-phenyl-urea (**13**)*

From intermediate **7d** (50 mg, 0.17 mmol) and phenyl isocyanate (2 eq) following the general procedure (24 h; purification by silica column, gradient c-Hex-EtOAc from 20–75% of EtOAc), the compound **13** was got (pale yellow solid, 46 mg, 65%); ^{1}H NMR (700 MHz, DMSO) δ 8.99 (s, 1H), 8.75 (s, 1H), 8.52 (dd, J = 4.7, 2.0 Hz, 1H), 8.34 (dd, J = 7.5, 2.0 Hz, 1H), 8.21 (s, 1H), 7.78 (dd, J = 10.9, 2.1 Hz, 1H), 7.74 (m, 1H), 7.51 (dd, J = 7.5, 4.8 Hz, 1H), 7.45 (d, J = 7.9 Hz, 2H), 7.28 (dd, J = 17.8, 9.9 Hz, 2H), 7.16 (dd, J = 8.9, 2.2 Hz, 1H), 7.12 (dd, J = 9.8, 4.5 Hz, 1H), 6.97 (dd, J = 20.5, 13.2 Hz, 1H), 6.46 (d, J = 1.7 Hz, 1H); LCMS (ESI): m/z 413.5 $[M+ H]^{+}$, Rt: 5.12 min.

*4.1.4. Synthesis of amides **16–19***

*4.1.4.1. N-(11-Oxo-10-pyridin-4-yl-10,11-dihydro-5-oxa-4,10-diaza-dibenzo[a,d] cyclohepten-7-yl)-2-phenyl-acetamide (**16**)*

To intermediate **7b** (40 mg, 0.131 mmol) in 1,4-dioxane (1.5 mL) were added K_2CO_3 (3 eq, 54 mg) and benzoyl chloride (1.5 eq, 23 μL). The mixture was stirred at rt for 1 h. The reaction mixture was partitioned in ethyl acetate and water. Layers were separated and the aqueous layer was extracted with ethyl acetate. The combined organic layers were dried (Na_2SO_4) and concentrated to render the crude product that was purified by silica flash chromatography (c-Hex-EtOAc from 10-80% of EtOAc) to afford **16** (white solid, 26 mg, 48%); ^{1}H NMR (300 MHz, DMSO) δ 10.48 (s, 1H), 8.72 (s, 2H), 8.55 (dd, J = 4.8, 2.0 Hz, 1H), 8.35 (dd, J = 7.6, 2.0 Hz, 1H), 8.10 (d, J = 2.4 Hz, 1H), 7.93 (m, 2H), 7.64-7.51 (m, 7H), 6.86 (d, J = 8.9 Hz, 1H); LCMS (ESI): m/z 409.2 $[M+ H]^+$, Rt: 3.69 min.

*4.1.4.2. N-(11-Oxo-10-pyridin-4-yl-10,11-dihydro-5-oxa-4,10-diaza-dibenzo[a,d] cyclohepten-7-yl)-benzamide (**17**)*

To intermediate **7b** (56 mg, 0.184 mmol) in 1,4-dioxane (2 mL) were added K_2CO_3 (3 eq, 76 mg) and phenylacetyl chloride (1.5 eq, 43 mg). The mixture was stirred at rt for 2 h. The reaction mixture was partitioned in ethyl acetate and water. Layers were separated. The organic phase was dried (Na_2SO_4) and concentrated to render the crude product that was purified by silica flash chromatography (c-Hex-EtOAc from 20−100% of EtOAc) to render **17** (white solid, 60 mg, 77%); ^{1}H NMR (300 MHz, DMSO) δ 10.42 (s, 1H), 8.70 (m, 2H), 8.51 (dd, J = 4.8, 2.0 Hz, 1H), 8.32 (dd, J = 7.6, 2.0 Hz, 1H), 7.93 (d, J = 2.3 Hz, 1H), 7.50 (m, 3H), 7.27 (m, 6H), 6.80 (d, J = 8.8 Hz, 1H), 3.63 (s, 2H); LCMS (ESI): m/z 423.1 $[M+ H]^+$, Rt: 3.78 min.

*4.1.4.3. 3,3,3-Trifluoro-2-hydroxy-2-methyl-N-(11-oxo-10-pyridin-4-yl-10,11-dihydro-5-oxa-4,10-diaza-dibenzo[a,d]cyclohepten-7-yl)-propionamide (**18**)*

To 2-(trifluoromethyl)-2-hydroxypropionic acid (1.5 eq, 39 mg, 0.246 mmol) in THF (1.5 mL) and DMAc (16 μL) at 0 ºC was added thionyl chloride (1.7 eq, 20 μL). The mixture (white suspension) was stirred at rt for 90 min and then intermediate **7b** (50 mg, 0.164 mmol) in THF (1.5 mL) was added. The reaction mixture was stirred at rt for 20 h and then it was heated at 70 ºC for 3 h. The reaction mixture was concentrated and the crude product was purified by silica flash chromatography (c-Hex-EtOAc from 20–100% of EtOAc). A second chromatography (DCM-MeOH from 0–15% of MeOH) was needed to render pure compound **18** (yellowish solid, 12 mg, 16%); ^{1}H NMR (300 MHz, DMSO) δ 10.27 (s, 1H), 8.77 (brs, 2H), 8.53 (dd, J = 4.8, 1.9 Hz, 1H), 8.34 (dd, J = 7.6, 2.0 Hz, 1H), 8.04 (d, J = 2.4 Hz, 1H), 7.54 (m, 5H), 6.81 (d, J = 8.9 Hz, 1H), 1.56 (s, 3H); LCMS (ESI): m/z 445.3 $[M+H]^{+}$, Rt: 3.45 min.

*4.1.4.4. 2-Hydroxy-2-methyl-N-(11-oxo-10-pyridin-4-yl-10,11-dihydro-5-oxa-4,10-diaza-dibenzo[a,d]cyclohepten-7-yl)-propionamide (**19**)*

To 2-hydroxyisobutyric acid (12 mg, 0.118 mmol) in THF (1 mL) and DMAc (10 μL) at 0 ºC was added thionyl chloride (1.5 eq, 11 μL). The mixture (cloudy aspect) was stirred at rt for 90 min and then intermediate **7a** (30 mg, 0.099 mmol) in THF (1 mL) was added. The reaction mixture was stirred at rt for 20 h and then it was heated at 70 ºC for 3 h. The solid in suspension was filtered and washed with ethyl acetate to render required product not pure. It was further purified by silica flash chromatography (c-Hex-EtOAc from 20–100%) yielding pure **19** (white solid, 4 mg, 10%) and a second batch less pure (15 mg); ^{1}H NMR (700 MHz, DMSO) δ 9.90 (s, 1H), 8.70 (dd, J = 7.9, 3.9 Hz, 2H), 8.53 (dd, J = 4.7, 2.0 Hz, 1H), 8.33 (dd, J = 7.5, 2.0 Hz, 1H), 8.08 (d, J = 2.3 Hz, 1H), 7.52 (m, 2H), 7.49 (dd, J = 4.7,

1.5 Hz, 2H), 6.78 (d, J = 8.9 Hz, 1H), 5.75 (s, 1H), 1.33 (s, 6H); LCMS (ESI): m/z 391.1 $[M+ H]^+$, Rt: 2.70 min.

*4.1.5. Synthesis of N-(11-Oxo-10-pyridin-4-yl-10,11-dihydro-5-oxa-4,10-diaza-dibenzo[a,d] cyclohepten-7-yl) -benzenesulfonamide (**20**)*

Intermediate **7b** (50 mg, 0.164 mmol) in pyridine (1.6 mL) at 0 ºC was treated with benzenesulfonyl chloride (1.5 eq, 31 μL). The orange reaction mixture was stirred at 0 ºC for 1 h. Ethanol (2 mL) was added and then concentrated. The crude product was purified by flash chromatography (c-Hex-EtOAc from 10–100% of EtOAc and then EtOAc-MeOH 0–15% since the product tended to precipitate in column) to render **20** (white solid, 65 mg, 89%); ^{1}H NMR (300 MHz, DMSO) δ 10.70 (s, 1H), 8.77 (brs, 2H), 8.52 (dd, J = 4.8, 2.0 Hz, 1H), 8.29 (dd, J = 7.6, 2.0 Hz, 1H), 7.76 (m, 2H), 7.56 (m, 3H), 7.47 (br s, 2H), 7.30 (m, 1H), 7.14 (d, J = 2.5 Hz, 1H), 6.91 (dd, J = 8.9, 2.5 Hz, 1H), 6.72 (d, J = 8.8 Hz, 1H); LCMS (ESI): m/z 445.2 $[M+ H]^+$, Rt: 3.62 min.

Acknowledgments

This research was supported in part by grant from the Spanish Ministry of Economy and Competitiveness (SAF2013-44267-R) and Spanish National Cancer Research Centre. F. J. García was supported by a Severo Ochoa FPI fellowship from the Spanish Ministry of Economy and Competitiveness.

Appendix A. Supplementary data

Scheme S1 and synthetic details of compound **15**, Figures S1-4, Tables S1-2, biological protocols and ^{1}H NMR spectra are detailed in the supporting information.

Notes

The authors declare no competing financial interest.

References

[1] Conaway, R. C.; Sato, S.; Tomomori-Sato, C.; Yao, T.; Conaway, J. W. The Mammalian Mediator Complex and Its Role in Transcriptional Regulation. *Trends Biochem. Sci.* **2005**, *30*, 250-255.

[2] Nemet, J.; Jelicic, B.; Rubelj, I.; Sopta, M. The two faces of Cdk8, a positive/negative regulator of transcription. *Biochimie* **2014**, *97*, 22-27.

[3] Li, N.; Fassl, A.; Chick, J.; Inuzuka, H.; Li, X.; Mansour, M. R.; Liu, L.; Wang, H.; King, B.; Shaik, S.; et al. Cyclin C Is a Haploinsufficient Tumour Suppressor. *Nat. Cell Biol.* **2014**, *16*, 1080-1091.

[4] Firestein, R.; Bass, A. J.; Kim, S. Y.; Dunn, I. F.; Silver, S. J.; Cuney, I.; Freed, E.; Ligon, A. H.; Vena,N.; Ogino, S.; et al. CDK8 Is a Colorectal Cancer Oncogene That Regulates Beta-Catenin Activity. *Nature* **2008**, *455*, 547-551.

[5] Firestein, R.; Shima, K.; Nosho, K.; Irahara, N.; Baba, Yl; Bojarski, E.; Giovannucci, E. L.; Hahn, W. C.; Fuchs, C. S.; Ogino, S. CDK8 Expression in 470 Colorectal Cancers in Relation to Beta-Catenin Activation, Other Molecular Alterations and Patient Survival. *Int. J. Cancer* **2010**, *126*, 2863-2873.

[6] Kapoor, A.; Goldberg, M. S.; Cumberland; L. K.; Ratnakumar, K.; Segura, M. F.; Emanuel, P. O.; Menendez, S.; Vardabasso, C.; Leroy, G.; Vidal, C. I.; Polsky, D.; Osman, I.; Garcia, B. A.; Hernando, E.; Bernstein, E. The Histone Variant macroH2A Suppresses Melanoma Progression Trough Regulation of CDK8. *Nature* **2010**, *468*, 1105-1109.

[7] Pelish, H.E.; Liau, B.B.; Nitulexcu, I.I.; Tangpeerachaikul, A.; Poss, Z. C.; Da Silva, D.H.; Caruso, B.T.; Arefolov. A.; Fadeyi, O.; Christie, A.L.; Du, K.; Banka, D.; Schneider, E.V.; Jestel. A.; Zou, G.; Si, C.; Ebmeier, C.C.; Bronson, R.T.; Krivstsov. A.V:; Myers, A.G.; Hohl, N.E.; Kung, A.L.; Armstrong, S.A.; Lemieus, M.E.; Taatjes, D.J.; Shair, M.D. Mediator kinase inhibition further activates super-enhancer-associated genes in AML. *Nature* **2015**, *526*, 273-276.

[8] Putz, E.M.; Gotthardt, D.; Hoermann, G. et al., CDK8-medited STAT1-S727 phosphorylation restrains NK cell cytotoxicity and tumor surveillance, Cell Rep. 2013, 437-444.

[9] Wilhelm, S.; Carter, C.; Lynch, M.; Lowinger, T.; Dumas, J.; Smith, R. A.; Schwartz, B.; Simantov, R.; Kelley, S. Discovery and development of sorafenib: a multikinase inhibitor for treating cancer. *Nature Reviews Drug Discovery* **2006**, *5*, 835-844.

[10] a) Porter, D. C.; Farmaki, E.; Altilia, S.; Schools, G. P.; West, D. K.; Chen, M.; Chang, B.; Puzyrev, A. T.; Lim, C.; Rokow-Kittell, R.; Friedhoff, L. T.; Papavassiliou, A. G.; Kalurupalle, S.; Hurteau, G.; Baran, P. S.; Gyorffy, B.; Wentland, M. P.; Broude, E. V.; Kiaris, H. and Ronninson, I. B. Cyclin-dependent kinase 8 mediates chemotherapy-induced tumor-promoting paracrine activities. *Proc*

Natl Acad Sci U S A. **2012**, *109,* 13799–13804. b) McDermott, S.J.M.; Chumanevich, A. A.; Lim, C.; Liang, J.; chen, M.; Altilia, S.; OLivr, D.; Rae, J. M.; Shtutman, M.; Kiaris, H.; Gyorffy, B.; Roninson, I. B.; Broude, E. V. Inhibition of CDK8 mediator kinase suppresses estrogen dependent transcription and the growth of estrogen receptor posititve breast cancer. *Oncotarget* **2017**, Feb 21;8(8):12558-12575.

[11] Dale, T.; Clarke, P.A.; Esdar, C.; Waalboer, D.; Adeniji-Popoola, O.; Ortiz-Ruiz, M.-J; Mallinger, A.; Samant, R.S.; Czodrowski, P.; Musil, D.; Schawarz, D.; Schenider, R.; Stubbs, M.; Ewan, K.; Fraser,E.; TePoele, R.; Court, W.; Box, G.; Valenti, M.; de Haven Brandon, A.; Gowan, S.; Rohdich, F.; Raynaud, F.; Schneider, R.; Poeschke, O.; Blaukat, A.; Workman, P.; Schiemann, K.; Wienke, D.; Blagg, J. A selective chemical probe for exploring the role of CDK8 and CDK19 in human disease. *Nat. Chem. Biol.* **2015**, *11*, 973-980.

[12] Cee, V. J.; Chen, D.; Lee, M. R.; Nicolaou, K. C. Cortistatin A is a High-Affinity Ligand of Protein Kinases ROCK, CDK8, and CDK11. *Angew. Chem. Int. Ed.* **2009**, *48*, 8952 –8957.

[13] Bergeron, P.; Koehler, M. F. T.; Blackwood, E. M.; Bowman, K.; Clark, K.; Firestein, R.; Kiefer, J. R.; Maskos, K.; McCleland, M. L.; Orren, L.; Ramaswamy, S.; Salphati, L.; Schmidt, S.; Schneider, E. V. Design and Development of a Series of Potent and Selective Type II Inhibitors of CDK8. *ACS Med. Chem. Lett.* **2016**, *7*, 223-228.

[14] Schneider, E. V., Böttcher, J., Blaesse, M.; Neumann, L.; Huber, R., Maskos, K. The Structure of CDK8/CycC Implicates Specificity in the CDK/Cyclin Family and Reveals Interaction with a Deep Pocket Binder. *J.Mol.Biol.* **2011**, *412*, 251-266.

[15] Schneider, E.V.; Böttcher, J.; Huber, R.; Maskos, K.; Neumann. L. Structure-kinetic relationship study of CDK8/CyCC specific compounds. *Proc Natl Acad Sci U S A.* **2013**, *110*, 8081–8086.

[16] Minimal energy conformations calculated with software from Pharmacelera.

[17] Meanwell, N. A. Synopsis of Some Recent Tactical Application of Bioisosteres in Drug Design. *J. Med. Chem.* **2011**, *54*, 2529-2591.

[18] Ohnmacht, C. J.; Russell, K.; Empfield, J. R.; Frank, C. A.; Gibson, K. H.; Mayhugh, D. R. et al. N-Aryl-3,3,3-trifluoro-2-hydroxy-2-methylpropanamides: KATP potassium channel openers. Modifications on the western region. *J. Med. Chem.* **1996**, *39*, 4592-4601

[19] PDB 6TPA. Purification, crystallization, data collection and refinement methods in supplementary material.

[20] . Selectivity Score is a quantitative measure of compound selectivity. It is calculated by dividing the number of kinases that compound bind to by the total number of distinct kinases tested, excluding mutant variants. S(35)= (number of non-mutant kinases with %Ctrl<35)/(number of non-mutant kinases tested). DiscoverX. https://www.discoverx.com/services/drug-discovery-development-services/kinase-profiling/kinomescan/scanmax.

[21] Davis, M.I.; Hunt, J.P.; Herrgard, S.; Ciceri, P.; Wodicka, L. M.; Pallares, G.; Hocker, M.; Treiber, D. K.; Zrrinkar, P. P. Comprehensive analysis of kinases inhibitor selectivity. *Nat. Biot.* **2011**, *29*, 1046-1051.

[22] Bancerek, J.; Poss, Z. C.; Steinparzer, I.; Sedlyarov, V.; Pfaffenwimmer, T.;Mikulic, I.; Dölken, L.; Strobl, B.; Müller, M.; Taatjes, D. J.; et al. CDK8 kinase phosphorylates transcription factor STAT1 to selectively regulate the interferon response. *Immunity* **2013**, *38*, 250-262.

[23] Klatt, F.; Leitner, A.; Kim, L. V.; Ho-Xuan, H.; Scheneider, E. V.; Langhammer, F.; Weinmann, R.; Müller, M.R.; Huber, R.; Meister, G.; Kuhn, C-D. A precisely positioned MED12 activation helix stimulates CDK8 kinase activity. *PNAS* **2020**, *117*, 6, 2894-2905.

[24] Li, Y.; Lu, X.; Ren. X.; Ding, K. Small Molecule Discoidin Domain Receptor Kinase Inhibitors and Potential Medical Applications *J. Med. Chem.* **2015**, *58*, 8, 3287-3301.

Highlights:

- Design of novel type II tricyclic CDK8 inhibitors based on Sorafenib.
- Binding of inhibitors to CDK8 by filling an unexplored cavity via displacement of its flexible P-loop.
- Potent and highly selective pyrido[2,3-b][1,5]benzoxazepin-5(6H)-one based CDK8 inhibitors.

Declaration of interests

☒ The authors declare that they have no known competing financial interests or personal relationships that could have appeared to influence the work reported in this paper.

☐The authors declare the following financial interests/personal relationships which may be considered as potential competing interests: